Multi-objective Topology Optimization Design of Micro-structures

Sebastián Miguel Giusti and Antonio André Novotny

Abstract This contribution proposes a methodology for the multi-objective synthesis and/or topology optimization of microstructures based on the topological derivative concept. The macroscopic properties are estimated by a standard multi-scale constitutive theory where the macroscopic responses are volume averages of their microscopic counterparts over a Representative Volume Element (RVE). We introduce a macroscopic cost functional that combines the mechanical and thermal effects in a single expression, allowing to design an RVE satisfying a specific thermo-mechanical macroscopic behavior. The algorithm is of simple computational implementation and relies in a level-set domain representation method. The effectiveness of the proposed methodology is illustrated by a set of finite element-based numerical examples.

1 Introduction

The accurate prediction of macroscopic thermal and mechanical properties of materials from the knowledge of their underlying microstructures has long been a subject of great interest in applied mechanics. The increasing understanding of the microscopic mechanisms responsible for the macroscopic response, allied to the industrial demand for more accurate predictive tools, led to the development and use of so-called *multiscale constitutive theories*. Such theories are currently a subject

S.M. Giusti (✉)
Departamento de Ingeniería Civil, Facultad Regional
Córdoba UTN/FRC - CONICET, Universidad Tecnológica Nacional,
Maestro M. López esq. Cruz Roja Argentina, X5016ZAA Córdoba, Argentina
e-mail: sgiusti@frc.utn.edu.ar

A.A. Novotny
Laboratório Nacional de Computação Científica LNCC/MCT,
Coordenação de Matemática Aplicada e Computacional, Av. Getúlio Vargas 333,
Petrópolis, RJ 25651-075, Brazil
e-mail: novotny@lncc.br

P.A. Muñoz-Rojas (ed.), *Computational Modeling, Optimization and Manufacturing Simulation of Advanced Engineering Materials*,
Advanced Structured Materials 49, DOI 10.1007/978-3-319-04265-7_2

of intensive research in applied mathematics and computational mechanics, whose mathematical roots can be traced back to the pioneers works [8, 13, 19, 20, 32].

Early applications were concerned with the description of relatively simple microscale phenomena often treated by analytical or semi-analytical methods [6, 7, 18, 27, 30]. More recent applications rely often on finite element-based computational simulations and are frequently applied to more complex material behavior [9, 25, 26, 31, 34].

One interesting branching of such developments is the study of the sensitivity of the macroscopic response to changes in the underlying microstructure. The sensitivity information becomes essential in the analysis and potential purpose-design and optimization of heterogeneous media. In the present work we adopt an approach that relies on exact formulae for the sensitivities of the macroscopic elastic and thermal responses to topological changes of the microscopic domain. These formulae have been derived in [16, 17]; and rely on the concepts of topological asymptotic analysis and topological derivative [33]—which provide the correct mathematical framework for the calculation of sensitivities under singular topological changes typical of microstructural optimization problems. The obtained sensitivities are given by a symmetric tensor field, of the same order that the constitutive operator, over the Representative Volume Element (RVE) that measures how the macroscopic constitutive parameters estimated within the multiscale framework changes when a small disk is introduced at the microscale. The final format of the proposed analytical formulae are strikingly simple and has been successfully applied to synthesis and optimization of elastic microstructures in [4, 10, 15].

In this work we introduce a macroscopic cost functional that combines the mechanical and thermal effects in a single expression. The associated topological derivative of each term of the cost functional has been respectively derived in [16, 17]. These results are used together with a level-set domain representation method in the synthesis and/or topology optimization of the RVE to achieve a specific thermo-mechanical macroscopic behavior. We claim however that the thermal-expansion effect is neglected, so that the resulting thermo-mechanical model is uncoupled.

The work is organized as follows. The multi-scale constitutive theories used in the estimation of the elastic and thermal macroscopic constitutive response is briefly described in Sect. 2. In Sect. 3 an overview of the topological derivative concept is given and the formulae for the topological derivatives of the macroscopic elasticity and thermal constitutive tensors relevant to the present context are presented. The topology optimization algorithm together with the numerical examples are presented in Sect. 4. Finally, some concluding remarks are made in Sect. 5.

2 Multi-objective Problem Formulation

Let $\Omega_\mu \subset \mathfrak{R}^2$ be an open and bounded domain defining a local Representative Volume Element (RVE) of the material. The domain of the sought optimal structure will be a subset of the hold-all domain Ω_μ. Therefore, given a RVE domain Ω_μ,

a general procedure for the topological design of multifunctional micro-structures consists in finding a subdomain $\omega_\mu \subset \Omega_\mu$ (the optimal structure domain) that solves the following constrained minimization problem:

$$\begin{cases} \underset{\omega_\mu \subset \Omega_\mu}{\text{Minimize}} & \mathscr{J}(\Omega_\mu) = \beta\, z(\mathbb{C}) + (1-\beta) h(\mathbf{K}), \\ \text{Subjected to} & |\omega_\mu| = V^*, \end{cases} \tag{1}$$

where the functional $\mathscr{J}(\Omega_\mu)$ is defined in the domain Ω_μ of the RVE. In the above definition, $h(\mathbf{K})$ and $z(\mathbb{C})$ are scalar functions depending on the constitutive thermal $\mathbf{K}$ and elastic $\mathbb{C}$ response tensors; and $\beta \in [0, 1]$ is the weighting coefficient for the multi-objective cost functional, which allows to control the contributions between the functions $h(\mathbf{K})$ and $z(\mathbb{C})$ on the objective function. By changing the weighting coefficient value from 0 through 1, we obtain a Pareto optimal set if it is convex. Finally, the required volume of the optimal domain at the end of the optimization process is denoted as V^*. The constitutive responses $\mathbf{K}$ and $\mathbb{C}$ are obtained from a variational approach in a constitutive multi-scale model. In the following sections, we briefly describe the adopted model to obtain these constitutive responses by a standard homogenization procedure.

2.1 Preliminaries in the Multi-scale Modeling

In this section we briefly describe the main concepts for a multi-scale constitutive analysis which allows to estimate the macroscopic constitutive tensors by using a homogenization-based variational framework with the complete description of a local RVE of the material. This constitutive modeling approach follows closely the strategy presented by [13, 25, 26], and whose variational structure is described in detail in the works [11, 12]. In this context, the main concept is the assumption that any point x of the macroscopic continuum $\Omega \subset \mathfrak{R}^2$ (refer to Fig. 1) is associated to a local RVE whose domain Ω_μ, with boundary $\partial\Omega_\mu$, has characteristic length L_μ, much smaller than the characteristic length L of the macro-continuum domain. For

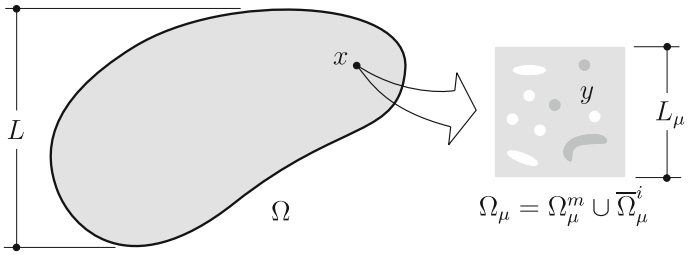

Fig. 1 Macroscopic continuum with a locally attached microstructure

simplicity, we consider that the RVE domain consist of a matrix Ω_μ^m, containing inclusions of different materials occupying a domain Ω_μ^i (see Fig. 1), but the formulation is completely analogous to the one presented here if the RVE contains voids instead. The total volume of the RVE is denoted as V_μ and contains the volume of all elements presented in the RVE, such as, solids phases and voids. Hereafter, symbols $(\cdot)_\mu$ denote quantities associated to the microscale.

2.2 The Homogenized Conductivity Tensor

In the context of the previous section we consider that at any arbitrary point $x \in \Omega$ the macroscopic temperature gradient $\nabla\theta$ is the volume average of the microscopic temperature gradient $\nabla\theta_\mu$:

$$\nabla\theta = \frac{1}{V_\mu}\int_{\Omega_\mu} \nabla\theta_\mu \tag{2}$$

where θ and θ_μ denote, respectively, the macroscopic and microscopic absolute temperature fields. As stated before, since we are in a thermomechanics setting in which the temperature itself has a physical relevance for the mechanical problem, we also consider the following homogenization formula for the temperature

$$\theta = \frac{1}{V_\mu}\int_{\Omega_\mu} \theta_\mu. \tag{3}$$

By making use of Green's theorem, we can promptly establish that the averaging relation (2) is equivalent to the following constraint on the temperature fields of the RVE:

$$\int_{\partial\Omega_\mu} \theta_\mu\, n \;=\; V_\mu\, \nabla\theta\,, \tag{4}$$

where n is the unit outward vector to $\partial\Omega_\mu$. Now, without loss of generality, the microscopic temperature field θ_μ can be split into a sum

$$\theta_\mu(y) = \theta + \overline{\theta}_\mu(y) + \widetilde{\theta}_\mu(y), \tag{5}$$

of a constant temperature field (coinciding with the macrosopic temperature $\theta(x)$), a homogeneous gradient temperature field, $\overline{\theta}_\mu(y) := \nabla\theta \cdot (y - y_o)$, and a temperature fluctuation field, $\widetilde{\theta}_\mu(y)$. In the definition of the field $\overline{\theta}_\mu(y)$, y_o is given by:

$$y_o = \frac{1}{V_\mu}\int_{\Omega_\mu} y\,. \tag{6}$$

Introducing the above splitting in (3) we obtain the following constraint for the microscopic temperature fluctuation field:

$$\int_{\Omega_\mu} \widetilde{\theta}_\mu = 0\,. \tag{7}$$

In view of the splitting (5), and taking into account constraints (2) and (3) we define the minimally constrained space of the admissible microscopic temperature fluctuation fields at the RVE as:

$$\Theta_\mu := \left\{ v \in H^1(\Omega_\mu) \,:\, \int_{\Omega_\mu} v = 0,\ \int_{\partial\Omega_\mu} v\, n = 0 \right\}. \tag{8}$$

Therefore, the resulting space of admissible variations of the microscopic temperature field at the RVE is also Θ_μ.

Following the split (5), the microscopic temperature gradient can be expressed as a sum

$$\nabla\theta_\mu = \nabla\theta + \nabla\widetilde{\theta}_\mu, \tag{9}$$

of a homogeneous gradient (uniform over the RVE) coinciding with the macroscopic temperature gradient and a field $\nabla\widetilde{\theta}_\mu$ corresponding to a fluctuation of the microscopic temperature gradient about the homogenized value.

Another fundamental concept underlying multiscale models of the present type is the *Hill-Mandel Principle of Macro-homogeneity*. Here, we shall assume the analogous relation for the thermal case [13, 17]

$$q \cdot \nabla\hat{\theta} = \frac{1}{V_\mu} \int_{\Omega_\mu} q_\mu(\theta_\mu) \cdot \nabla\hat{\theta}_\mu \quad \forall(\nabla\hat{\theta}, \hat{\theta}_\mu) \text{ kinematically admissible} \tag{10}$$

where $q_\mu(\theta_\mu)$ denotes the microscopic heat flux associated to the microscopic temperature θ_μ and q is its macroscopic counterpart.

Equation (10) plays a crucial role in the formulation of thermal constitutive models within the present framework since it provides the variational principle that governs the scale bridging for the thermal problem. The main consequences of the application of that principles are:

- Micro-thermal equilibrium problem: given the macroscopic temperature θ and the macroscopic temperature gradient $\nabla\theta$, find the temperature fluctuation field $\widetilde{\theta}_\mu \in \Theta_\mu$ such that

$$\int_{\Omega_\mu} q_\mu(\theta_\mu) \cdot \nabla\eta = 0 \quad \forall\eta \in \Theta_\mu. \tag{11}$$

- Characterization of the macroscopic heat flux: given the macroscopic temperature θ, its gradient $\nabla\theta$, and θ_μ—the solution of problem (11), compute q as

$$q = \frac{1}{V_\mu} \int_{\Omega_\mu} q_\mu(\theta_\mu). \tag{12}$$

In the present analysis, we shall assume the materials of the RVE matrix and inclusions to satisfy the classical Fourier constitutive law:

$$q_\mu(\xi) = -\mathbf{K}_\mu \nabla \xi \,, \tag{13}$$

where $\mathbf{K}_\mu$ is the thermal conductivity tensor defined at the RVE level. The isotropic representation of this tensor is given by

$$\mathbf{K}_\mu = k_\mu \mathrm{I} \,, \tag{14}$$

being I used to denote the second order identity tensors and k_μ the thermal conductivity parameter (scalar value). The linearity of (13) together with the additive decomposition (5), allows the microscopic thermal flux field to be split as

$$q_\mu(\theta_\mu) = -\mathbf{K}_\mu \nabla \theta - \mathbf{K}_\mu \nabla \widetilde{\theta}_\mu \,. \tag{15}$$

By introducing decomposition (15) into the thermal equilibrium equation (11), we obtain the closed form of the microscopic thermal equilibrium problem: given $\nabla\theta$, find $\widetilde{\theta}_\mu \in \Theta_\mu$ such that

$$\int_{\Omega_\mu} \mathbf{K}_\mu \nabla \widetilde{\theta}_\mu \cdot \nabla \eta = -\int_{\Omega_\mu} \mathbf{K}_\mu \nabla \theta \cdot \nabla \eta \quad \forall \eta \in \Theta_\mu. \tag{16}$$

Crucial to the developments of the multi-scale model for the thermal problem, is the derivation of formulae for the macroscopic thermal conductivity tensor. This is addressed in the following.

From the additive split of the microscopic temperature field (5) and by using the homogenization procedure, we have that the macroscopic thermal conductivity tensor can be obtained as a sum

$$\mathbf{K} = \overline{\mathbf{K}} + \widetilde{\mathbf{K}}, \tag{17}$$

of a homogenized (volume average) macroscopic thermal conductivity tensor $\overline{\mathbf{K}}$, given by,

$$\overline{\mathbf{K}} = \frac{1}{V_\mu} \int_{\Omega_\mu} \mathbf{K}_\mu \,, \tag{18}$$

and a contribution $\widetilde{\mathbf{K}}$ associated to the solution of the problem (16), defined as:

$$\widetilde{\mathbf{K}} := \left[\frac{1}{V_\mu} \int_{\Omega_\mu} (q_\mu(\widetilde{\theta}_{\mu_j}))_i \right] e_i \otimes e_j \,, \tag{19}$$

where $(q_\mu(\widetilde{\theta}_{\mu_j}))_i$ is the ith component of the microscopic fluctuation flux field associated with the temperature fluctuation field $\widetilde{\theta}_{\mu_j}$; being the scalar fields $\widetilde{\theta}_{\mu_j} \in \mathscr{V}_\mu$ the solutions of the linear variational equations

$$\int_{\Omega_\mu} q_\mu(\widetilde{\theta}_{\mu_j}) \cdot \nabla\eta = -\int_{\Omega_\mu} \mathbf{K}_\mu e_j \cdot \nabla\eta \quad \forall\eta \in \mathscr{V}_\mu. \tag{20}$$

for $j = 1, 2$ (in the two-dimensional case). For a more detailed description on the derivation of the above expressions, we refer the reader to [17, 25].

2.3 The Homogenized Elasticity Tensor

Using the concept of *homogenization* we define the macroscopic strain tensor ε at a point x of the macroscopic continuum as the volume average of its microscopic counterpart ε_μ over the domain of the RVE. For this work, we consider that the microscopic strain field ε_μ is given by the symmetric part of the gradient of the microscopic displacement field u_μ. Then, the macroscopic strain tensor is written as:

$$\varepsilon := \frac{1}{V_\mu} \int_{\Omega_\mu} \nabla^s u_\mu \, . \tag{21}$$

Tacking into account the Green formula in the above definition we obtain the following equivalent expression for the homogenized (macroscopic) strain tensor ε

$$\varepsilon = \frac{1}{V_\mu} \int_{\partial\Omega_\mu} u_\mu \otimes_s n \, , \tag{22}$$

where n is the outward unit normal to the boundary $\partial\Omega_\mu$ and $\otimes_s$ denotes the symmetric tensor product of vectors. Note that, the above expression imposes a kinematical constraint over the admissible displacement fields over the RVE such that the kinematical homogenization principle (21) is satisfied. Now, without loss of generality, it is possible split u_μ into a sum

$$u_\mu(y) = u + \overline{u}_\mu(y) + \widetilde{u}_\mu(y) \, , \tag{23}$$

of a constant (rigid) RVE displacement coinciding with the macro displacement $u(x)$, a field $\overline{u}_\mu(y) := \varepsilon(y - y_o)$ and a fluctuation displacement field $\widetilde{u}_\mu(y)$ (See Fig. 2). With the above split, the microscopic strain field can be written as a sum

$$\nabla^s u_\mu = \varepsilon + \nabla^s \widetilde{u}_\mu \, , \tag{24}$$

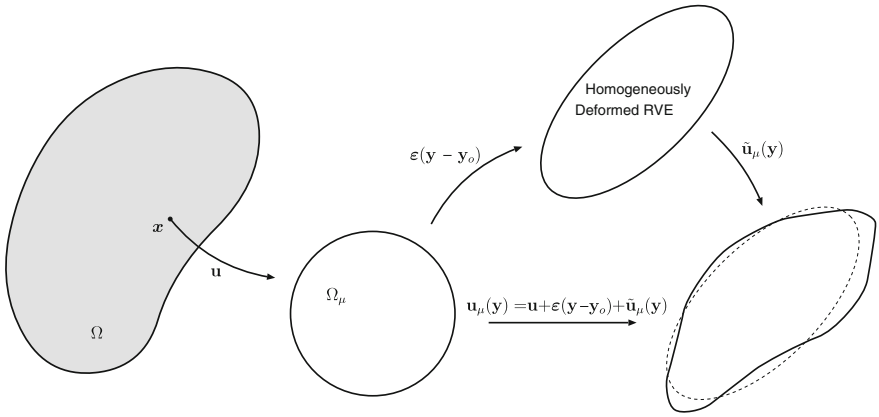

Fig. 2 Additive splitting of the microscopic displacement field

of a homogeneous strain (uniform over the RVE) coinciding with the macroscopic strain and a field $\nabla^s \widetilde{u}_\mu$ corresponding to a fluctuation of the microscopic strain about the homogenized (average) value. We also assume the following constraint on the microscopic displacement field u_μ

$$u = \frac{1}{V_\mu} \int_{\partial\Omega_\mu} u_\mu \, . \tag{25}$$

By introducing the additive splitting for the microscopic displacement field u_μ into the above constraint, we obtain the following expression for the microscopic displacement fluctuation field

$$\int_{\partial\Omega_\mu} \widetilde{u}_\mu = 0 \, . \tag{26}$$

In this sense, the kinematical homogenization procedure introduced in (21) induces the *minimally constrained space of admissible microscopic displacement fluctuation fields* at the RVE

$$\mathscr{U}_\mu := \left\{ v \in H^1(\Omega_\mu, \mathfrak{R}^n) \, : \, \int_{\Omega_\mu} v = 0, \int_{\partial\Omega_\mu} v \otimes_s n = 0 \right\} . \tag{27}$$

Hence, the space of kinematically admissible variations of the microscopic displacement field at the RVE is $\mathscr{U}_\mu$ as well.

As in the thermal case, the physical bridging between macro and micro scales is provided by the Hill-Mandel Principle of Macro-homogeneity [20, 24], which is

$$\sigma \cdot \hat{\varepsilon} := \frac{1}{V_\mu} \int_{\Omega_\mu} \sigma_\mu(u_\mu) \cdot \nabla^s \hat{u}_\mu \ , \quad \forall (\hat{u}_\mu, \hat{\varepsilon}) \text{ kinematically admissible.} \tag{28}$$

where $\sigma_\mu(u_\mu)$ denotes the microscopic stress associated to the microscopic displacement u_μ and σ is its macroscopic counterpart.

As before, using standard variational arguments, the Hill-Mandel principle provides two consequences: the microscopic mechanical equilibrium problem and the homogenization formula for the Cauchy stress.

- Micro-mechanical equilibrium problem: given the macroscopic strain ε, find the microscopic displacement fluctuation field $\widetilde{u}_\mu \in \mathscr{U}_\mu$ such that

$$\int_{\Omega_\mu} \sigma_\mu(u_\mu) \cdot \nabla^s \eta = 0 \quad \forall \eta \in \mathscr{U}_\mu \ . \tag{29}$$

- Characterization of the macroscopic stress: given the macroscopic strain ε, and $\widetilde{u}_\mu$—the solution of problem (29)—, compute σ as

$$\sigma := \frac{1}{V_\mu} \int_{\Omega_\mu} \sigma_\mu(u_\mu) \ . \tag{30}$$

For this work, materials that satisfy the classical linear elastic constitutive law will be used to describe the behavior of the RVE matrix and inclusions. That is, the microscopic stress tensor field $\sigma_\mu(\xi)$ satisfies

$$\sigma_\mu(\xi) = \mathbb{C}_\mu \nabla^s \xi \ , \tag{31}$$

where $\mathbb{C}_\mu$ is the classical fourth order elasticity tensor. In addition, we assume that the matrix and the inclusion are isotropic and homogeneous materials, thus $\mathbb{C}_\mu$ is defined as:

$$\mathbb{C}_\mu = \frac{E_\mu}{1 - \nu_\mu^2} \left[\left(1 - \nu_\mu\right) \mathbb{I} + \nu_\mu \left(\mathrm{I} \otimes \mathrm{I}\right) \right] \ , \tag{32}$$

with E_μ and ν_μ denoting, respectively, the Young's moduli and the Poisson's ratio of the domain Ω_μ. Moreover, in (32) we use $\mathbb{I}$ to denote the fourth order identity tensor.

The linearity of (31) together with the additive decomposition (24), allows the microscopic stress field to be split as

$$\sigma_\mu(u_\mu) = \sigma_\mu(\overline{u}_\mu) + \sigma_\mu(\widetilde{u}_\mu) \ , \tag{33}$$

where $\sigma_\mu(\overline{u}_\mu)$ is the stress field associated with the uniform strain induced by $\overline{u}\,(y)$ and $\sigma_\mu(\widetilde{u}_\mu)$ is the stress fluctuation field associated with $\widetilde{u}_\mu\,(y)$.

In view of expressions (29)–(33), we have that the *RVE mechanical equilibrium problem* consists of finding, for a given macroscopic strain ε, an admissible microscopic displacement fluctuation field $\widetilde{u}_\mu \in \mathscr{U}_\mu$, such that

$$\int_{\Omega_\mu} \sigma_\mu(\widetilde{u}_\mu) \cdot \nabla^s \eta = -\int_{\Omega_\mu} \sigma_\mu(\overline{u}_\mu) \cdot \nabla^s \eta \quad \forall \eta \in \mathscr{U}_\mu \,. \tag{34}$$

In the constitutive multi-scale model previously introduced, was presented how to use the macroscopic information (strain tensor ε) to obtain the microscopic displacement field u_μ. In this context, by using the same concepts it is possible to obtain a closed form of the macroscopic constitutive response, in our case, the homogenized elasticity tensor $\mathbb{C}$. This methodology, suggested by [25], is based on re-writing the problem (34) as a superposition of linear problems associated with the individual Cartesian components of the macroscopic strain tensor. Then, the macroscopic (homogenized) tensor $\mathbb{C}$ can be written as a sum

$$\mathbb{C} = \overline{\mathbb{C}} + \widetilde{\mathbb{C}} \,, \tag{35}$$

of an homogenized (volume average) macroscopic elasticity tensor $\overline{\mathbb{C}}$, given by

$$\overline{\mathbb{C}} = \frac{1}{V_\mu} \int_{\Omega_\mu} \mathbb{C}_\mu \,, \tag{36}$$

and a contribution $\widetilde{\mathbb{C}}$ associated to the choice of space $\mathscr{U}_\mu$, defined as:

$$\widetilde{\mathbb{C}} := \left[\frac{1}{V_\mu} \int_{\Omega_\mu} (\sigma_\mu(\widetilde{u}_{\mu_{kl}}))_{ij} \right] \left(e_i \otimes e_j \otimes e_k \otimes e_l \right) \,, \tag{37}$$

where $(\sigma_\mu(\widetilde{u}_{\mu_{kl}}))_{ij}$ is the ijth component of the fluctuation stress field associated with the fluctuation displacement field $\widetilde{u}_{\mu_{kl}}$; being the vector fields $\widetilde{u}_{\mu_{kl}} \in \mathscr{U}_\mu$ the solutions of the linear variational equations

$$\int_{\Omega_\mu} \sigma_\mu(\widetilde{u}_{\mu_{kl}}) \cdot \nabla^s \eta = -\int_{\Omega_\mu} \mathbb{C}_\mu(e_k \otimes e_l) \cdot \nabla^s \eta \quad \forall \eta \in \mathscr{U}_\mu \,, \tag{38}$$

for $k, l = 1, 2$ (in the two-dimensional case). After solving the set of variational problems (38), the full microscopic displacement field $u_{\mu_{kl}}$ can be obtained using the eq. (23) for each canonical direction $\{e_k, e_l\}$. For a more detailed description on the derivation of expressions (35)–(38) we refer the reader to [12, 16, 25].

3 Topological Derivative

In this section we present the topological derivative concept used to devise a topology design algorithm of micro-structures, within the multi-scale framework introduced in the previous section. The concept of topological sensitivity analysis, rigorously

introduced by Sokołowski and Żochowsky in 1999 [33], allows to obtain asymptotic expansions of shape functionals defined over a given domain, when a singular perturbation is introduced in an arbitrary point changing the topology of the (original) domain. The notion of topological derivative has proved extremely useful in the treatment of a wide range of problems in mechanics, optimization, inverse analysis and image processing and has become a subject of intensive research in the last years, see for instance, the works [1, 5, 15, 16, 21, 22, 35] and the book [29].

Now, let ψ be a functional that depends on a given domain and let it have sufficient regularity so that the following expansion is possible

$$\psi(\rho) = \psi(0) + f(\rho)\, T_D\psi + o(f(\rho)) \ , \tag{39}$$

where $\psi(0)$ is the functional evaluated in the original domain and $\psi(\rho)$ denotes the functional for the topologically perturbed domain. The parameter ρ defines the size of the topological perturbation, so that the original domain is retrieved when $\rho = 0$. In addition, $f(\rho)$ is a *function* such that $f(\rho) \to 0$ with $\rho \to 0^+$ and $o(f(\rho))$ contains all terms of higher order in $f(\rho)$. The term $T_D\psi$ of (39) is defined as the *topological derivative* of ψ at the unperturbed (original) RVE domain. Thus, the topological derivative can be seen as a first order correction factor over $\psi(0)$ to approximate $\psi(\rho)$. In fact, rearranging (39) and taking the limit $\rho \to 0^+$, we have the definition of the topological derivative

$$T_D\psi(\hat{x}) = \lim_{\rho \to 0^+} \frac{\psi(\rho(\hat{x})) - \psi(0)}{f(\rho)} \ . \tag{40}$$

In this work we will use a closed formula for the sensitivity of the homogenized constitutive response (17) and (35) to the introduction of a circular inclusion centered at an arbitrary point of the RVE domain. To present this formula it is appropriate to define the topologically perturbed RVE by a small inclusion of radius ρ represented by $\mathscr{B}_\rho$. More precisely, the perturbed domain is obtained when a circular hole $\mathscr{B}_\rho$ of radius ρ is introduced at an arbitrary point $\hat{y} \in \Omega_\mu$. Next, this region is replaced with the circular inclusion with different material property (refer to Fig. 3). In the presence of the perturbation described above, the microscopic constitutive tensors are given by

$$\mathbb{C}_\mu^\rho = \begin{cases} \mathbb{C}_\mu \ in \ \Omega_\mu \backslash \overline{\mathscr{B}_\rho} \\ \gamma \mathbb{C}_\mu \ in \ \mathscr{B}_\rho \end{cases} \quad \text{and} \quad \mathbf{K}_\mu^\rho = \begin{cases} \mathbf{K}_\mu \ in \ \Omega_\mu \backslash \overline{\mathscr{B}_\rho} \\ \gamma \mathbf{K}_\mu \ in \ \mathscr{B}_\rho \end{cases} \ , \tag{41}$$

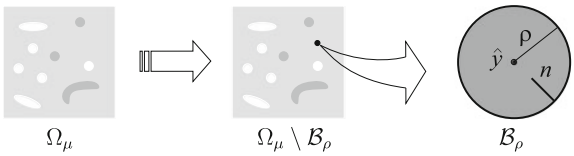

Fig. 3 Topological perturbation at the microscopic level

where the scalar parameter $\gamma \in \Re^+$ is defined as the contrast parameter between the constitutive responses of the domains $\Omega_\mu \backslash \overline{\mathscr{B}_\rho}$ and $\mathscr{B}_\rho$.

In view of the previous description of the topologically perturbed RVE domain, we can state the following results:

Theorem 1 *The topological asymptotic expansion of the macroscopic elasticity tensor associated to the topologically perturbed RVE domain, namely $\mathbb{C}^\rho$, is written as*

$$\mathbb{C}^\rho = \mathbb{C} + \frac{\pi\rho^2}{V_\mu} T_D\mathbb{C} + o(\rho^2)\,, \tag{42}$$

where the fourth order topological derivative tensor $T_D\mathbb{C}$ is given by

$$T_D\mathbb{C} = \mathbb{H}_\mu \sigma_\mu(u_{\mu_{ij}}) \cdot \sigma_\mu(u_{\mu_{kl}})\,(e_i \otimes e_j \otimes e_k \otimes e_l)\,. \tag{43}$$

Some terms in the above formula require explanation. The canonical stress tensors $\sigma_\mu(u_{\mu_{ij}})$ are given by

$$\sigma_\mu(u_{\mu_{ij}}) = \mathbb{C}_\mu(e_i \otimes e_j) + \sigma_\mu(\widetilde{u}_{\mu_{ij}}) \tag{44}$$

where $\widetilde{u}_{\mu_{ij}}$ are the solutions to the set of canonical variational problems presented in (38)*. In addition, the isotropic fourth order tensor $\mathbb{H}_\mu$ is defined as*

$$\mathbb{H}_\mu = -\frac{1}{E_\mu}\left(\frac{1-\gamma}{1+a\gamma}\right)\left[4\mathbb{I} - \frac{1-\gamma(a-2b)}{1+b\gamma}\,(\mathrm{I}\otimes\mathrm{I})\right], \tag{45}$$

with the parameters a and b given by

$$a = \frac{1+\nu_\mu}{1-\nu_\mu} \quad \textit{and} \quad b = \frac{3-\nu_\mu}{1+\nu_\mu}\,. \tag{46}$$

Proof The reader interested in the proof of this theorem may refer to [4, 16].

Theorem 2 *The topological asymptotic expansion of the macroscopic thermal conductivity tensor associated to the topologically perturbed RVE domain, namely $\mathbf{K}^\rho$, is written as*

$$\mathbf{K}^\rho = \mathbf{K} + \frac{\pi\rho^2}{V_\mu} T_D\mathbf{K} + o(\rho^2)\,, \tag{47}$$

where the second order topological derivative tensor $T_D\mathbf{K}$ is given by

$$T_D\mathbf{K} = -2k_\mu \frac{1-\gamma}{1+\gamma} \nabla\theta_{\mu_i} \cdot \nabla\theta_{\mu_j}\,(e_i \otimes e_j)\,, \tag{48}$$

being $\nabla\theta_{\mu_i}$ *the canonical microscopic temperature gradient fields given by*

$$\nabla\theta_{\mu_i} = \nabla\theta \cdot e_i + \widetilde{\theta}_{\mu_i}, \tag{49}$$

with the scalars $\widetilde{\theta}_{\mu_i}$ *representing the solutions of the set of canonical variational problems* (20).

Proof The reader interested in the proof of this theorem may refer to [17].

Remark 1 The topological derivatives $T_D\mathbb{C}$ and $T_D\mathbf{K}$, presented in Eqs. (43) and (48), exactly measures the sensitivity of the constitutive operators $\mathbb{C}$ and $\mathbf{K}$ when a new material (characterized by a singular perturbation) is introduced at an arbitrary point of the RVE domain. This information is of paramount importance for the designer in order to produce a material-by-design for an specific application.

The optimization procedure presented in (1) can be alternatively written as the following unconstrained minimization problem:

$$\underset{\omega_\mu \subset \Omega_\mu}{\text{Minimize}} \;\; J(\Omega_\mu) = \beta\, z(\mathbb{C}) + (1-\beta) h(\mathbf{K}) + \lambda \frac{\left|\omega_\mu\right|}{V_\mu}\,, \tag{50}$$

where λ is a fixed Lagrange multiplier associated to a volume constraint over ω_μ. Since the topological sensitivity is a derivative with respect to the volume fraction of the perturbation, then, we can apply directly the rules of differential calculus. Thus, according to the topological asymptotic expansion of the homogenized constitutive response given by Eqs. (42) and (47), the topological derivative of the cost function $J(\Omega_\mu)$ can be obtained by using the chain rule. Therefore, it comes

$$T_D J = \beta \left\langle Dz(\mathbb{C}), T_D(\mathbb{C}) \right\rangle + (1-\beta) \left\langle Dh(\mathbf{K}), T_D(\mathbf{K}) \right\rangle + \lambda\,. \tag{51}$$

where the term $\langle Dh(\mathbf{K}), T_D(\mathbf{K})\rangle$ and $\langle Dz(\mathbb{C}), T_D(\mathbb{C})\rangle$ should be understood as the derivatives of the functions $h(\mathbf{K})$ and $z(\mathbb{C})$ with respect to the tensor $\mathbf{K}$ or $\mathbb{C}$ in the direction of $T_D\mathbf{K}$ or $T_D\mathbb{C}$, respectively. Also, note that the brackets $\langle\cdot,\cdot\rangle$ denotes the appropriate product between the derivatives of any function $h(\mathbf{K})$ or $z(\mathbb{C})$ and the corresponding topological derivative $T_D\mathbf{K}$ or $T_D\mathbb{C}$.

We use this simple idea to devise a topology algorithm for the synthesis and optimization of multi-purpose micro-structures based on the minimization/maximization of cost functions defined in terms of homogenized properties. In order to fix theses ideas, let us present four examples concerning the topological derivatives of given functions $h(\mathbf{K})$ and $z(\mathbb{C})$. For Let $\varphi_1, \varphi_2 \in \mathbb{R}^n \times \mathbb{R}^n$ be any pair of second order tensors, and $\phi_1, \phi_2 \in \mathbb{R}^n$ be any pair of vectors. Then we obtain the following results:

Example 1 We consider a function $h(\mathbf{K})$ of the form

$$h(\mathbf{K}) := \mathbf{K}\phi_1 \cdot \phi_2\,. \tag{52}$$

Therefore, by performing the derivation as indicated previously, its topological derivative is given by

$$\langle Dh(\mathbf{K}), T_D(\mathbf{K})\rangle = T_D(\mathbf{K})\phi_1 \cdot \phi_2 \, . \tag{53}$$

If we set $\phi_1 = e_i$ and $\phi_2 = e_j$, for instance, we get $h(\mathbf{K}) = (\mathbf{K})_{ij}$ and its topological derivative is given by $(T_D(\mathbf{K}))_{ij}$. It means that the product $\langle Dh(\mathbf{K}), T_D(\mathbf{K})\rangle$ actually represents the topological derivative of the component $(\mathbf{K})_{ij}$ of the homogenized thermal conductivity tensor $\mathbf{K}$.

Example 2 Now, we consider an objective function $h(\mathbf{K})$ of the form

$$h(\mathbf{K}) := \mathbf{K}^{-1}\phi_1 \cdot \phi_2 \, . \tag{54}$$

In order to perform the derivative, note that we can differentiate the relation $\mathbf{K}\mathbf{K}^{-1} = \mathbf{I}$ with respect to the volume fraction of the perturbation in the RVE, namely

$$T_D(\mathbf{K})\mathbf{K}^{-1} + \mathbf{K}T_D(\mathbf{K}^{-1}) = 0 \, . \tag{55}$$

After multiplying to the left by $\mathbf{K}^{-1}$ we get

$$\mathbf{K}^{-1}T_D(\mathbf{K})\mathbf{K}^{-1} + T_D(\mathbf{K}^{-1}) = 0 \, , \tag{56}$$

which leads to

$$T_D(\mathbf{K}^{-1}) = -\mathbf{K}^{-1}T_D(\mathbf{K})\mathbf{K}^{-1} \, . \tag{57}$$

Thus, the topological derivative of $h(\mathbf{K})$ is given by

$$\langle Dh(\mathbf{K}), T_D(\mathbf{K})\rangle = -(\mathbf{K}^{-1}T_D(\mathbf{K})\mathbf{K}^{-1})\phi_1 \cdot \phi_2 \, . \tag{58}$$

Note that by setting tensors ϕ_1 and ϕ_2 properly, we can obtain the topological derivative in its explicit form of any component of the inverse of the homogenized elasticity tensor $\mathbf{K}^{-1}$.

Example 3 Let us consider an objective function $h(\mathbf{K})$ of the form

$$h(\mathbf{K}) := \frac{1}{2}\mathbf{K}^{-1} \cdot \mathbf{I} \, . \tag{59}$$

By taking into account the result previously obtained, the topological derivative of $h(\mathbf{K})$ is given by

$$\langle Dh(\mathbf{K}), T_D(\mathbf{K})\rangle = -\frac{1}{2}(\mathbf{K}^{-1}T_D(\mathbf{K})\mathbf{K}^{-1}) \cdot \mathbf{I} \, . \tag{60}$$

Example 4 Finally, we consider a function $z(\mathbb{C})$ of the form

$$z(\mathbb{C}) := \mathbb{C}^{-1}\varphi_1 \cdot \varphi_2 \,. \tag{61}$$

By using the same methodology as the previous example, the corresponding topological derivative can be written as

$$\langle Dz(\mathbb{C}), T_D(\mathbb{C})\rangle = -(\mathbb{C}^{-1}T_D(\mathbb{C})\mathbb{C}^{-1})\varphi_1 \cdot \varphi_2 \,. \tag{62}$$

Again, note that by setting tensors φ_1 and φ_2 properly, we can obtain the topological derivative in its explicit form of any component of the inverse of the homogenized elasticity tensor $\mathbb{C}^{-1}$.

In the next section, the optimization problem stated in (50) is solved by using the level-set-based algorithm devised in [3], which was also successfully applied in the context of microstructure topology optimization in the works [4, 10]. It relies on a level-set domain representation and the topological derivative (51) is used as a feasible descent direction. As cost functions for the multi-objective optimization problem will be used a combinations of the functions presented above. For other type of cost function in this context see the works [4, 10, 28].

4 Numerical Results

The numerical solution of the minimization problem (50) is undertaken here by the algorithm proposed in [3] in conjunction with the finite element approximation of the multiscale boundary value problems (20) and (38) proposed in [14]. The algorithm relies essentially on an optimality criterion based on the topological derivative of the objective function and on a level-set representation of the structure domain. For completeness, the algorithm is outlined in the following. For further details we refer to the works [3, 5].

With the level-set representation, the current optimized domain ω_μ is characterized by a level-set function $\psi \in L^2(\Omega_\mu)$ as

$$\omega_\mu = \{x \in \Omega_\mu, \psi(x) < 0\} \,, \tag{63}$$

and its complement as

$$\Omega_\mu \backslash \overline{\omega}_\mu = \{x \in \Omega_\mu, \psi(x) > 0\} \,. \tag{64}$$

To devise a level-set-based algorithm whose aim is to produce a optimal topology that satisfies (50) it is convenient to define the function

$$g(x) = \begin{cases} -T_D J(x) \text{ if } \psi(x) < 0 \\ T_D J(x) \text{ if } \psi(x) > 0 \end{cases} . \tag{65}$$

Here it should be noted that a negative (positive) value of the topological derivative $T_D J(x)$ at a point $x \in \Omega_\mu$ indicates that the introduction of an infinitesimal inclusion centered at that point of the RVE produces a perturbed domain whose objective functional value is smaller (greater) than that of the original domain. Then, according to [3], a sufficient condition of local optimality in this context is that

$$T_D J(x) > 0 \quad \forall x \in \Omega_\mu . \tag{66}$$

That is, no infinitesimal inclusion in Ω_μ can cause a reduction in the value of the objective functional.

The present algorithm relies on the fact that, in view of definition (65), a sufficient condition for (66) to holds is

$$\exists\, \tau > 0 \quad \text{s.t} \quad g = \tau\, \psi , \tag{67}$$

or, equivalently,

$$\theta := \arccos \left[\frac{\langle g, \psi \rangle_{L^2(\Omega_\mu)}}{\|g\|_{L^2(\Omega_\mu)} \, \|\psi\|_{L^2(\Omega_\mu)}} \right] = 0 , \tag{68}$$

where θ is the angle between the vectors g and ψ in $L^2(\Omega_\mu)$. The algorithm itself aims to generate a sequence $\{\psi_i\}$ of level set functions (a sequence of microstructural domains $\{\omega_{\mu_i}\}$) that will produce for some iteration n a domain ω_{μ_n} such that (68) is satisfied to within a given small numerical tolerance $\varepsilon_\theta > 0$:

$$\theta_n = \arccos \left[\frac{\langle g_n, \psi_n \rangle_{L^2(\Omega_\mu)}}{\|g_n\|_{L^2(\Omega_\mu)} \, \|\psi_n\|_{L^2(\Omega_\mu)}} \right] \leq \varepsilon_\theta . \tag{69}$$

The procedure starts with the choice of an initial guess for the optimal domain, i.e. with the choice of a starting level-set function $\psi_0 \in L^2(\Omega_\mu)$. With $\mathscr{S}$ denoting the unit sphere in $L^2(\Omega_\mu)$, the algorithm is explicitly given by

$$\begin{aligned} &\psi_0 \in \mathscr{S} , \\ &\psi_{i+1} = \frac{1}{\sin\theta_i} \left[\sin((1-\kappa_i)\theta_i)\Psi_i + \sin(\kappa_i \theta_i) \frac{g_i}{\|g_i\|_{L^2(\Omega_\mu)}} \right] , \end{aligned} \tag{70}$$

where i denotes a generic iteration number and $\kappa_i \in [0, 1]$ is a step size determined by a line-search in order to decrease the value of the objective function $T_D J$. The iterative process is stopped when for some iteration the step size κ_i is smaller than a given numerical tolerance $\varepsilon_\kappa > 0$:

$$\kappa_i < \varepsilon_\kappa \ . \tag{71}$$

That is, when the topology is effectively no longer changing with the iterations. If, at this stage, the optimality condition (69) is not satisfied to the desired degree of accuracy, i.e. if

$$\theta_i > \varepsilon_\theta \ , \tag{72}$$

then a uniform mesh refinement of the hold-all RVE domain Ω_μ is carried out and the iterative procedure is continued.

In the computation of $T_D J$ according to expression (50) the topological derivatives are first computed within the finite elements (at Gauss points) and then extrapolated to nodes. The final discretized version of the field $T_D J$ used in the iterations is generated by the finite element shape functions with smoothed nodal values obtained in a standard fashion. The level-set functions ψ and the discretized field $T_D J$ are generated by the same shape functions used in the finite element approximation of the boundary value problems (20) and (38). The material properties are assigned to nodes of the mesh depending on whether they are at points with $\psi < 0$ or $\psi > 0$. In this way, elements crossed by the interface (defined by $\psi = 0$) will have material properties obtained by a standard interpolation of the nodal values of these properties using the element shape functions. Obviously, according to the above procedure, the resolution of the optimal RVE domain depends directly on the fineness of the adopted mesh.

The effectiveness of the algorithm described above is demonstrated in the next numerical examples. These examples are related to the synthesis of microstructures in order to meet a specified macroscopic behavior. The optimization procedure is conducted by considering the RVE constituted in a bi-material fashion, i.e. the matrix part and the voids.

We start by fixing the RVE geometry, which is represented by the unity square $\Omega_\mu = (0, 1) \times (0, 1)$. The level-set initialization is given by a circular disc, with radius $r = 0.25$, centered in the RVE at point (0.5, 0.5)—with the origin of the Cartesian coordinate system located at the bottom left hand corner of the RVE, see Fig. 4.

For the conduction cases, the thermal conductivity associated to the microstructure is given by $k_\mu = 1$. The constitutive properties for the elasticity case are Young's modulus $E_\mu = 1$ and Poisson ratio $\nu_\mu = 0.3$. For both cases, the parameter γ is the same and equal to 0.01. The inclusion with constitutive properties given by γk_μ and γE_μ is used in the topology design to mimic the void part of the RVE. To solve the multi-scale variational problems (20) and (38) we consider periodic boundary condition [32].

In all cases, the initial mesh is structured as shown in Fig. 4, with 3281 nodes and 6400 three-noded triangular elements. Although the algorithm converges on the initial mesh in each case to the prescribed accuracy of $\varepsilon_\theta = 1°$, we perform some uniform refinements in order to improve the final result. The final mesh contains 205441 nodes and 409600 elements. In all figures presented in this section, the black color represent the matrix part of the RVE optimal domain ω_μ and the white color is used to mimic the void part of the domain.

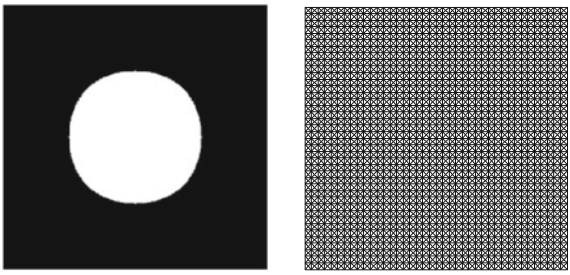

Fig. 4 Initial guess (*left*) and initial mesh (*right*)

4.1 Example 1. Bulk Modulus and Horizontal Conductivity Maximization

In this first example, we wish to maximize the macroscopic thermal conductivity in the direction e_1 (horizontal direction) and the bulk modulus simultaneously. Accordingly we use the objective function $h(\mathbf{K})$ and $z(\mathbb{C})$ defined by Eqs. (54) and (61), respectively. For this case we choose $\phi_1 = \phi_2 = e_1$ and $\varphi_1 = \varphi_2 = \mathbf{I}$. The Lagrange multiplier is taken as $\lambda = 10.0$. The resulting optimized topologies for three values of parameter β are shown in Fig. 5. The obtained RVEs have a volume of 40 % of the initial volume. The macroscopic constitutive properties of the results are presented in Table 1.

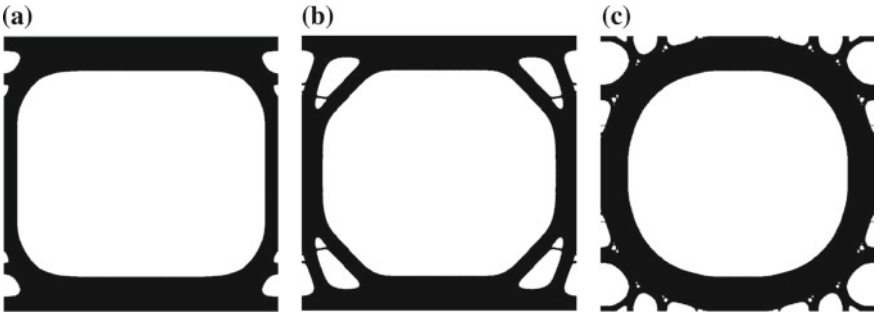

Fig. 5 Example 1. Bulk modulus and horizontal conductivity maximization. **a** $\beta = 0.25$, **b** $\beta = 0.50$, **c** $\beta = 0.75$

Table 1 Example 1

β	0.25	0.50	0.75
Bulk modulus (K)	0.115	0.131	0.140
Conductivity k_{11}	0.273	0.273	0.268
Conductivity k_{22}	0.143	0.204	0.242

Effective properties

From the previous results, the influence of the weighting parameter β is evident. When this parameter decreases, the microstructure tends to promote the thermal conductivity in the direction of e_1 maintaining the bulk modulus in a low value. Moreover, for low values of β the differences between the conductivities k_{11} and k_{22} increases. The topology obtained for the higher values of β are very similar to the one analyzed by Hashin and Shtrikman [19]. These authors obtained microstructures known as *coated spheres assemblages* or *Hashin-Shtrikman micro-structures* that provide lower and upper bounds for the elastic properties of bi-material composites.

4.2 Example 2. Bulk Modulus and Orthogonal Conductivity Maximization

The aim of this example is to show the topology of the RVE that maximize the bulk modulus and the conductivity in two orthogonal directions (coinciding with e_1 and e_2). Therefore, we define the objective function $J(\Omega_\mu)$ by using the functions $h(\mathbf{K})$ and $z(\mathbb{C})$ defined by Eqs. (59) and (61), respectively. For this case we choose again $\varphi_1 = \varphi_2 = \mathbf{I}$. For a Lagrange multiplier $\lambda = 10.0$, the resulting optimized topologies for three value of parameter β are shown in Fig. 6. The effective (or macroscopic) properties are presented in Table 2.

The obtained RVEs have a volume of 40 % of the initial volume. Due to the definition of the objective functional $h(\mathbf{K})$, the RVEs are completely symmetric with

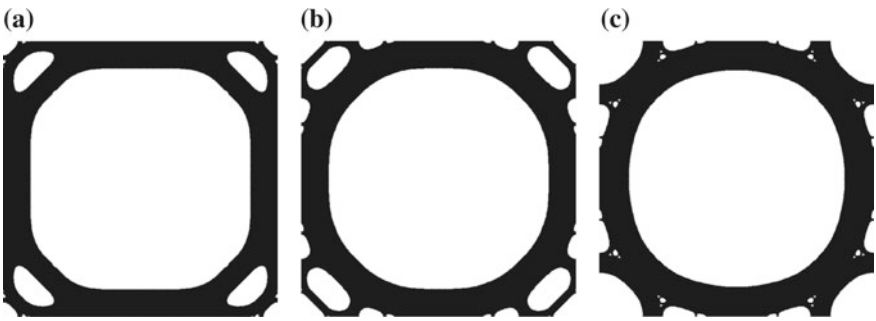

Fig. 6 Example 2. Bulk modulus and orthogonal conductivity maximization. **a** $\beta = 0.25$, **b** $\beta = 0.50$, **c** $\beta = 0.75$

Table 2 Example 2

β	0.25	0.50	0.75
Bulk modulus (K)	0.129	0.131	0.137
Conductivity k_{11}	0.236	0.239	0.250
Conductivity k_{22}	0.236	0.239	0.250

Effective properties

respect the two axis parallel to e_1 and e_2; and the conductivities in these directions have the same value (for each β). As in the previous example, the Bulk modulus of the microstructure increases with the values of the parameter β. The conductivities shown the same trend as the bulk modulus K. This behavior can be explained as following. The maximization of the bulk modulus implies in obtaining of a microstructure whose internal structure is aligned in two orthogonal directions. On the other hand, the maximization of the conductivity implies in the same kind of RVE. Therefore, these two goals of the optimization procedure involve the same type of internal arrangement of the microstructural elements in the RVE. Similar to the previous examples, the topology obtained for $\beta = 0.75$ are very similar to the one analyzed by Hashin and Shtrikman [19]. They consist of disks of the most compliant material coated with rings of stiffer material (bi-material composites).

4.3 Example 3. Poisson's Ratio and Horizontal Conductivity Maximization

The goal of the optimization procedure for this example is obtain a microstructure whose macroscopic the Poisson's ratio and conductivity in the direction of e_1 are maximums. To this ends, we use the objective function $h(\mathbf{K})$ and $z(\mathbb{C})$ defined by Eqs. (54) and (61), respectively. Here, we choose $\phi_1 = \phi_2 = e_1$ and $\varphi_1 = e_1 \otimes e_1$ and $\varphi_2 = e_2 \otimes e_2$. The Lagrange multiplier is taken as $\lambda = 1.0$. The results of the optimization procedure for three value of parameter β are shown in Fig. 7, and the macroscopic constitutive properties are presented in Table 3.

The obtained RVEs have a volume of around of the 20 % of the initial volume. The higher value of Poisson's ratio was obtained for the lower value of parameter β and in the same direction as the higher conductivity. This effect is due to the contribution of the function $h(\mathbf{K})$ to the mechanical part in the objective function $J(\Omega_\mu)$. We observe here that for the three value of the weighting coefficient β, the synthesized microstructure exhibit at the end of the optimization procedure has a *pantograph-like*

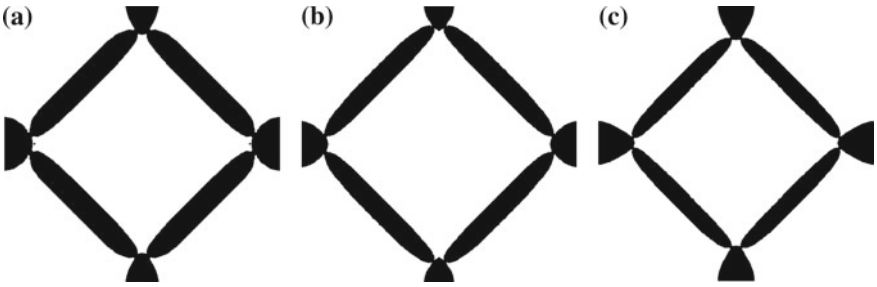

Fig. 7 Example 3. Poisson ratio and horizontal conductivity maximization. **a** $\beta = 0.25$, **b** $\beta = 0.50$, **c** $\beta = 0.75$

Table 3 Example 3

β	0.25	0.50	0.75
Poisson ratio ν_{12}	0.803	0.810	0.789
Poisson ratio ν_{21}	0.841	0.811	0.787
Conductivity k_{11}	0.112	0.095	0.082
Conductivity k_{22}	0.104	0.092	0.081

Effective properties

topology. This type of microstructure allows a maximum transfer of strain energy from one direction to the direction orthogonal to it.

4.4 Example 4. Poisson's Ratio Minimization and Horizontal Conductivity Maximization

In this example, we wish to promote the macroscopic conductivity in the direction of e_1 and minimize the Poisson's ratio. Accordingly we use the objective function $h(\mathbf{K})$ and $z(\mathbb{C})$ defined by Eqs. (54) and (61), respectively. For this case where we choose $\phi_1 = \phi_2 = e_1$ and $\varphi_1 = e_1 \otimes e_1$ and $\varphi_2 = -e_2 \otimes e_2$. The Lagrange multiplier is taken as $\lambda = 1.0$ and the resulting optimized topologies for three value of parameter β are shown in Fig. 8. The macroscopic constitutive properties are presented in Table 4.

The obtained final volume of the topologies presented in Fig. 8 are of around of the 45 % of the initial volume. For all cases, and as consequence of the optimization procedure, the obtained microstructures exhibit negative values for the macroscopic Poisson's ratio. In the following we present the homogenized fourth-order elasticity tensors for the topologies of Fig. 8.

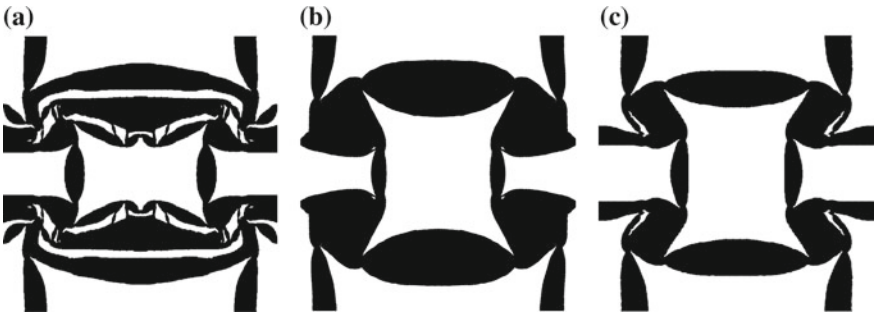

Fig. 8 Example 4. Poisson ratio minimization and horizontal conductivity maximization. **a** $\beta = 0.25$, **b** $\beta = 0.50$, **c** $\beta = 0.75$

Table 4 Example 4

β	0.25	0.50	0.75
Poisson ratio ν_{12}	−0.289	−0.376	−0.439
Poisson ratio ν_{21}	−0.511	−0.482	−0.475
Conductivity k_{11}	0.265	0.214	0.139
Conductivity k_{22}	0.111	0.141	0.128

Effective properties

$$\begin{aligned}
\mathbb{C}|_{\beta=0.25} &= \begin{pmatrix} 0.1256 & -0.0364 & 0.0 \\ -0.0364 & 0.0713 & 0.0 \\ 0.0 & 0.0 & 0.0096 \end{pmatrix}, \\
\mathbb{C}|_{\beta=0.50} &= \begin{pmatrix} 0.1064 & -0.0401 & 0.0 \\ -0.0401 & 0.0830 & 0.0 \\ 0.0 & 0.0 & 0.0105 \end{pmatrix}, \\
\mathbb{C}|_{\beta=0.75} &= \begin{pmatrix} 0.0788 & -0.0346 & 0.0 \\ -0.0346 & 0.0728 & 0.0 \\ 0.0 & 0.0 & 0.0075 \end{pmatrix}.
\end{aligned} \tag{73}$$

When the value of β decreases the differences in the behavior in the two orthogonal direction are more evident. This effect as been analyzed in the previous examples and the conclusion presented there remain valid here as well.

The best value for a negative Poisson's ratio was obtained for a parameter $\beta = 0.25$ for the same direction where the conductivity is maximized. Also, for the same value of β the internal arrangement of the microstructure is more complex than higher values of the parameter. The results show that, regardless of the particular values of β used in the objective functional $J(\Omega_\mu)$, the optimized microstructure features the auxetic behavior of the star-shaped encapsulated inclusions analyzed, among others, in [2, 23]. This type of micro-cell is known as *nonconvex-shaped* or *re-entrant corner* microstructures.

4.5 Example 5. Poisson Ratio Minimization and Orthogonal Conductivity Maximization

Similar to the previous example, here the goal is to minimize the macroscopic Poisson's ratio and the conductivity in two orthogonal directions (coinciding with e_1 and e_2). Therefore, in the definition of the objective function $J(\Omega_\mu)$ we consider the functions $h(\mathbf{K})$ and $z(\mathbb{C})$ given by Eqs. (59) and (61), respectively. Again we choose $\varphi_1 = e_1 \otimes e_1$ and $\varphi_2 = -e_2 \otimes e_2$. For the optimization procedure, a Lagrange multiplier $\lambda = 1.0$ is used. The resulting optimized topologies for several values of

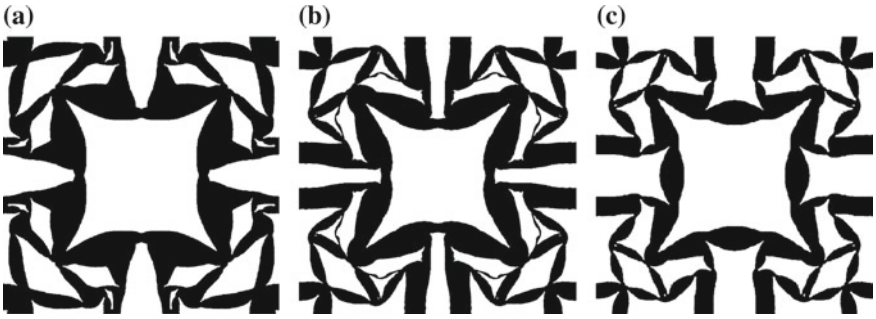

Fig. 9 Example 5. Poisson ratio minimization and orthogonal conductivity maximization. **a** $\beta = 0.25$, **b** $\beta = 0.50$, **c** $\beta = 0.75$

Table 5 Example 5

β	0.25	0.50	0.75
Poisson ratio ν_{12}	−0.403	−0.421	−0.425
Poisson ratio ν_{21}	−0.403	−0.421	−0.425
Conductivity k_{11}	0.195	0.169	0.138
Conductivity k_{22}	0.195	0.169	0.138

Effective properties

parameter β are shown in Fig. 9 and the effective constitutive properties are presented in Table 5.

The obtained final volume of the topologies presented in Fig. 9 are of around of the 50 % of the initial volume. As in the previous example, the obtained microstructures exhibit negative values for the macroscopic Poisson's ratio. For this case, the value of the Poisson's ratio in the two orthogonal directions are the same. This behavior is due to the symmetry imposed to the results by the objective functional $h(\mathbf{K})$. In the following we present the homogenized fourth-order elasticity tensors for the topologies of Fig. 9.

$$\begin{aligned}
\mathbb{C}|_{\beta=0.25} &= \begin{pmatrix} 0.0983 & -0.0397 & 0.0 \\ -0.0397 & 0.0983 & 0.0 \\ 0.0 & 0.0 & 0.0215 \end{pmatrix}, \\
\mathbb{C}|_{\beta=0.50} &= \begin{pmatrix} 0.0939 & -0.0396 & 0.0 \\ -0.0396 & 0.0939 & 0.0 \\ 0.0 & 0.0 & 0.0163 \end{pmatrix}, \\
\mathbb{C}|_{\beta=0.75} &= \begin{pmatrix} 0.0795 & -0.0338 & 0.0 \\ -0.0338 & 0.0795 & 0.0 \\ 0.0 & 0.0 & 0.0099 \end{pmatrix}.
\end{aligned} \tag{74}$$

The value of the Poisson's ratios decreases (more negative) when the weighting coefficient β is higher. In fact, when the contribution of the functional $z(\mathbb{C})$ is higher, the objective functional $J(\Omega_\mu)$ tends to promote a mechanical response instead of a conductivity. Here, the results also show that the optimized microstructure features the auxetic behavior analyzed, among others, in [2, 23]. This type of micro-cell is known as *nonconvex-shaped* or *re-entrant corner* microstructures.

4.6 Example 6. Shear Modulus and Horizontal Conductivity Maximization

For this last example, the aim is to show the topology of the RVE that maximize the macroscopic conductivity in the direction e_1 and the Shear modulus simultaneously. Therefore, the definition of the objective functions $h(\mathbf{K})$ and $z(\mathbb{C})$ given by Eqs. (54) and (61), respectively, will be used. For the complete definition of the functions $h(\mathbf{K})$ and $z(\mathbb{C})$, we choose $\phi_1 = \phi_2 = e_1$ and $\varphi_1 = \varphi_2 = e_1 \otimes e_2 + e_2 \otimes e_1$. The minimization of the present function $z(\mathbb{C})$ corresponds to the maximization of the effective shear modulus G. The Lagrange multiplier is taken as $\lambda = 5.0$. The resulting optimized topologies for three value of parameter β are shown in Fig. 10 and the effective constitutive properties are presented in Table 6.

The obtained final volume of the topologies presented in Fig. 10 are of around of the 40 % of the initial volume. Notice that the highest values of the macroscopic

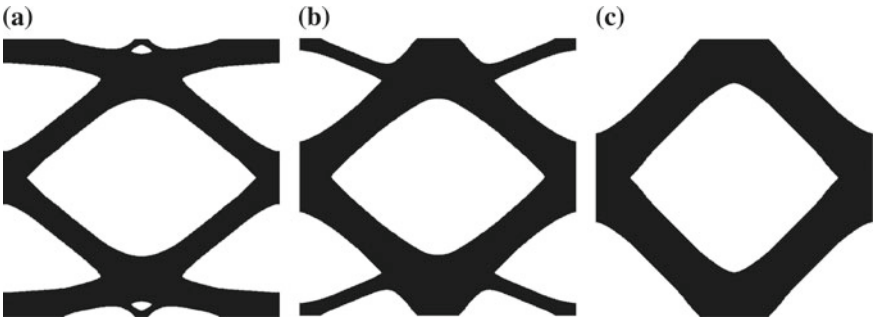

Fig. 10 Example 6. Shear modulus and horizontal conductivity maximization. **a** $\beta = 0.25$, **b** $\beta = 0.50$, **c** $\beta = 0.75$

Table 6 Example 6

β	0.25	0.50	0.75
Shear modulus G	0.084	0.109	0.117
Conductivity k_{11}	0.362	0.339	0.280
Conductivity k_{22}	0.160	0.227	0.262

Effective properties

shear modulus G is obtained when the parameter β increases. Independently of the parameter β, the main structure of the RVE is composed by four bars in a rhomboidal arrangement. To promote the conductivity in the direction e_1, for lower values of β, the microstructure develop bars in that direction, see Fig. 10a, b. With this arrangement the conductivity in the direction of e_1 increases.

5 Concluding Remarks

A multi-objective topology design of periodic microstructures procedure has been proposed. This procedure is based on the concept of topological derivative and a level-set domain representation method. For the optimization problem, a cost functional was constructed in order to archive simultaneously a specific macroscopic elastic and thermal behavior. The homogenized elasticity and conductivity tensors are estimated by a well-established multi-scale constitutive theory in which the macroscopic response are obtained as the volume averages of their microscopic counterparts over a RVE. The analytical topological derivatives of the constitutive responses are tensor fields of the same order that the constitutive tensors. To deal with a specific macroscopic behavior, scalar functions depending on the elasticity and thermal tensors were defined. The topological derivative of these functions are obtained through the direct application of conventional rules of differential calculus. These features have been explored in the minimization/maximization of cost functions defined in terms of homogenized properties. The proposed procedure was successfully and efficiently used in several numerical examples of optimum topology design of microstructures. We remark that the methodology presented here is of simple implementation in a material-by-design engineering or industrial application.

References

1. Allaire, G., Jouve, F., Van Goethem, N.: Damage and fracture evolution in brittle materials by shape optimization methods. J. Comput. Phys. **230**(12), 5010–5044 (2011)
2. Almgreen, R.F.: An isotropic three-dimensional structure with Poisson's ratio–1. J. Elast. **15**(4), 427–430 (1985)
3. Amstutz, S., Andrä, H.: A new algorithm for topology optimization using a level-set method. J. Comput. Phys. **216**(2), 573–588 (2006)
4. Amstutz, S., Giusti, S.M., Novotny, A.A., de Souza Neto, E.A.: Topological derivative for multi-scale linear elasticity models applied to the synthesis of microstructures. Int. J. Numer. Methods Eng. **84**, 733–756 (2010)
5. Amstutz, S., Novotny, A.A., de Souza Neto, E.A.: Topological derivative-based topology optimization of structures subject to Drucker-Prager stress constraints. Comput. Methods Appl. Mech. Eng. **233–236**, 123–136 (2012)
6. Auriault, J.L.: Effective macroscopic description for heat conduction in periodic composites. Int. J. Heat Mass Transf. **26**(6), 861–869 (1983)
7. Auriault, J.L., Royer, P.: Double conductivity media: a comparison between phenomenological and homogenization approaches. Int. J. Heat Mass Transf. **36**(10), 2613–2621 (1993)

8. Bensoussan, A., Lions, J.L., Papanicolau, G.: Asymptotic Analysis for Periodic Microstructures. North Holland, Amsterdam (1978)
9. Celentano, D.J., Dardati, P.M., Godoy, L.A., Boeri, R.E.: Computational simulation of microstructure evolution during solidification of ductile cast iron. Int. J. Cast Met. Res. **21**(6), 416–426 (2008)
10. de Souza Neto, E.A., Amstutz, S., Giusti, S.M., Novotny, A.A.: Topology optimization design of micro-structures considering different multi-scale models. Comput. Model. Eng. Sci. **62**(1), 23–56 (2010)
11. de Souza Neto, E.A., Feijóo, R.A.: On the equivalence between spatial and material volume averaging of stress in large strain multi-scale solid constitutive models. Mech. Mater. **40**(10), 803–811 (2008)
12. de Souza Neto, E.A., Feijóo, R.A.: Variational foundations of large strain multiscale solid constitutive models: kinematical formulation. In: Advanced Computational Materials Modeling: From Classical to Multi-Scale Techniques. Wiley-VCH Verlag GmbH & Co. KGaA, Weinheim, Germany (2011)
13. Germain, P., Nguyen, Q.S., Suquet, P.: Continuum thermodynamics. J. Appl. Mech. Trans. ASME **50**(4), 1010–1020 (1983)
14. Giusti, S.M., Blanco, P.J., de Souza Neto, E.A., Feijóo, R.A.: An assessment of the Gurson yield criterion by a computational multi-scale approach. Eng. Comput. **26**(3), 281–301 (2009)
15. Giusti, S.M., Novotny, A.A., de Souza Neto, E.A.: Sensitivity of the macroscopic response of elastic microstructures to the insertion of inclusions. In: Proceeding of the Royal Society A: Mathematical, Physical and Engineering Sciences, vol. 466, pp. 1703–1723 (2010)
16. Giusti, S.M., Novotny, A.A., de Souza Neto, E.A., Feijóo, R.A.: Sensitivity of the macroscopic elasticity tensor to topological microstructural changes. J. Mech. Phys. Solids **57**(3), 555–570 (2009)
17. Giusti, S.M., Novotny, A.A., de Souza Neto, E.A., Feijóo, R.A.: Sensitivity of the macroscopic thermal conductivity tensor to topological microstructural changes. Comput. Methods Appl. Mech. Eng. **198**(5–8), 727–739 (2009)
18. Gurson, A.L.: Continuum theory of ductile rupture by void nucleation and growth: part I—yield criteria and flow rule for porous ductile media. J. Eng. Mater. Technol. Trans. ASME **99**(1), 2–15 (1977)
19. Hashin, Z., Shtrikman, S.: A variational approach to the theory of the elastic behaviour of multiphase materials. J. Mech. Phys. Solids **11**(2), 127–140 (1963)
20. Hill, R.: A self-consistent mechanics of composite materials. J. Mech. Phys. Solids **13**(4), 213–222 (1965)
21. Hintermüller, M., Laurain, A.: Multiphase image segmentation and modulation recovery based on shape and topological sensitivity. J. Math. Imaging Vis. **35**, 1–22 (2009)
22. Hintermüller, M., Laurain, A., Novotny, A.A.: Second-order topological expansion for electrical impedance tomography. Adv. Comput. Math. **36**(2), 235–265 (2012)
23. Lakes, R.: Foam structures with negative Poisson's ratio. Sci. AAAS **235**(4792), 1038–1040 (1987)
24. Mandel, J.: Plasticité Classique et Viscoplasticité. CISM Lecture Notes. Springer, Udine (1971)
25. Michel, J.C., Moulinec, H., Suquet, P.: Effective properties of composite materials with periodic microstructure: a computational approach. Comput. Methods Appl. Mech. Eng. **172**(1–4), 109–143 (1999)
26. Miehe, C., Schotte, J., Schröder, J.: Computational micro-macro transitions and overall moduli in the analysis of polycrystals at large strains. Comput. Mater. Sci. **16**(1–4), 372–382 (1999)
27. Nemat-Nasser, S., Hori, M.: Micromechanics: Overall Properties of Heterogeneous Materials. North-Holland, Amsterdam (1993)
28. Novotny, A.A.: Topological derivative for multi-scale linear elasticity models in three spatial dimensions. Optimization of Structures and Components. Advanced Structured Materials, vol. 43. Springer, Switzerland (2013)
29. Novotny, A.A., Sokołowski, J.: Topological Derivatives in Shape Optimization. Interaction of Mechanics and Mathematics. Springer, Berlin (2013)

30. Ostoja-Starzewski, M., Schulte, J.: Bounding of effective thermal conductivities of multiscale materials by essential and natural boundary conditions. Phys. Rev. B **54**(1), 278–285 (1996)
31. Oyen, M.L., Ferguson, V.L., Bembey, A.K., Bushby, A.J., Boyde, A.: Composite bounds on the elastic modulus of bone. J. Biomech. **41**(11), 2585–2588 (2008)
32. Sanchez-Palencia, E.: Non-homogeneous Media and Vibration Theory. Lecture Notes in Physics, vol. 127. Springer, Berlin (1980)
33. Sokołowski, J., Żochowski, A.: On the topological derivative in shape optimization. SIAM J. Control Optim. **37**(4), 1251–1272 (1999)
34. Speirs, D.C.D., de Souza Neto, E.A., Perić, D.: An approach to the mechanical constitutive modelling of arterial tissue based on homogenization and optimization. J. Biomech. **41**(12), 2673–2680 (2008)
35. Van Goethem, N., Novotny, A.A.: Crack nucleation sensitivity analysis. Math. Methods Appl. Sci. **33**(16), 197–1994 (2010)

http://www.springer.com/978-3-319-04264-0

Computational Modeling, Optimization and Manufacturing Simulation of Advanced Engineering Materials

Muñoz-Rojas, P.A. (Ed.)
2016, VIII, 393 p. 215 illus., 87 illus. in color., Hardcover
ISBN: 978-3-319-04264-0